Published in final edited form as:
Vet Pathol. 2014 July ; 51(4): 846–857. doi:10.1177/0300985813501335.

Phenotypic Characterization of the KK/HlJ Inbred Mouse Strain

A. Berndt[1], **B. A. Sundberg**[2], **K. A. Silva**[2], **V. E. Kennedy**[2], **M. A. Richardson**[1], **Q. Li**[3], **R. T. Bronson**[2], **J. Uitto**[3], and **J. P. Sundberg**[2]

[1]Department of Medicine, University of Pittsburgh, Pittsburgh, PA, USA

[2]The Jackson Laboratory, Bar Harbor, ME, USA

[3]Department of Dermatology and Cutaneous Biology, Jefferson Medical College, Philadelphia, PA, USA

Abstract

Detailed histopathological diagnoses of inbred mouse strains are important for interpreting research results and defining novel models of human diseases. The aim of this study was to histologically detect lesions affecting the KK/HlJ inbred strain. Mice were examined at 6, 12, and 20 months of age and near natural death (ie, moribund mice). Histopathological lesions were quantified by percentage of affected mice per age group and sex. Predominant lesions were mineralization, hyperplasia, and fibro-osseous lesions. Mineralization was most frequently found in the connective tissue dermal sheath of vibrissae, the heart, and the lung. Mineralization was also found in many other organs but to a lesser degree. Hyperplasia was found most commonly in the pancreatic islets, and fibro-osseous lesions were observed in several bones. The percentage of lesions increased with age until 20 months. This study shows that KK/HlJ mice demonstrate systemic aberrant mineralization, with greatest frequency in aged mice. The detailed information about histopathological lesions in the inbred strain KK/HlJ can help investigators to choose the right model and correctly interpret the experimental results.

Keywords

systemic mineralization; ectopic mineralization; PXE model; KK/HlJ mice; vibrissae dermal sheath

Inbred strains of mice have important implications as model systems for human diseases and, as such, contribute to our current understanding of biology and pathology more than any other mammalian system. Laboratory mice originated by selective inbreeding for particular traits (eg, coat color or hair loss), which were of importance to the early mouse fanciers.[31] In the past century, disease susceptibilities similar to those in humans were found for many inbred mouse strains, yet this was often guided by the investigator's interest in a

Corresponding Author: J. P. Sundberg, The Jackson Laboratory, 600 Main St, Bar Harbor, ME 04609-1500, USA. john.sundberg@jax.org.

Declaration of Conflicting Interests
The author(s) declared no potential conflicts of interest with respect to the research, authorship, and/or publication of this article.

certain disease process or organ system. By focusing on a specific lesion or organ, other strain-specific aberrations, which may also be influential to the trait of interest, can easily be overlooked. System-wide histopathological analysis of individual inbred strains can not only uncover unknown traits, which help to explain research observations, but also identify novel disease models.

The origins of the KK/HlJ inbred mouse strain dates back to 1944, when K. Kondo obtained Nishiki-nezumi Japanese fancy mice in Kasukabe and started inbreeding KK substrains.[33] The currently available KK/HlJ mice that are distributed by The Jackson Laboratory (Bar Harbor, ME) have been inbred for more than 64 generations and were obtained from the Herberg Laboratory at the Diabetes Research Institute in Germany.[12] KK substrains are often used for studying the metabolic syndrome because of their inherited glucose intolerance and insulin resistance, which result in hyperglycemia.[12] KK/HlJ mice have a strong tendency to develop type 2 diabetes (T2D) in response to certain dietary regimens (eg, high-fat diet) and aging.[14] Diabetic nephropathy (characterized by increased kidney weight, albuminuria, and proteinuria), [25,26] interstitial fibrotic heart lesions,[29] and corneal degeneration[13,21] accompany the hyperglycemia if not treated by therapeutic interventions.

In addition to T2D susceptibility, the KK/HlJ strain is susceptible to aging-related vascular mineralization in the heart and kidney, and this characteristic may contribute to their “presensitized” state to develop albuminuria in response to chronic hyperglycemia.[18] This strain has been proposed as a spontaneous model for human pseudoxanthoma elasticum (PXE) because of mineralization of the vibrissa sheath combined with systemic mineralization.[5,20] KK/HlJ mice have also been used for studying aging-related hearing loss due to its homozygosity for a mutation in cadherin 23 (otocadherin; Cdh23), which causes a progressive impairment of hearing starting at 10 months of age.[39] Finally, this strain exhibits the most severe naive airway hyperresponsiveness among 36 tested inbred and wild-derived strains. KK/HlJ mice were more responsive than commonly used genetic models for airway hyperresponsiveness, such as the A/J strain.[3,19]

The purpose of this investigation was to determine and quantify histopathological lesions systemically in aging KK/HlJ mice. Cross-sectional (6, 12, and 20 months of age) and longitudinal studies (moribund mice, close to natural death at 14–28 months of age) were performed to identify the frequency of lesions across several organs. This study provides a comprehensive overview on background diseases in KK/HlJ that will allow investigators to interpret experimental data and, potentially, to choose this strain as a novel model for human and other mammalian diseases.

Materials and Methods

Mice

All KK/HlJ mice (JR #2106) were part of a large-scale aging study by The Jackson Aging Center, for which details have been described elsewhere.[35] Briefly, mice were obtained, raised, and maintained at the breeding facilities of The Jackson Laboratory. At age of 6 to 8 weeks, mice were transferred from the breeding facilities to a specific pathogen-free room and assigned to cross-sectional and longitudinal groups, which were set up in parallel. Mice

in the cross-sectional groups were euthanized at 6 (201–210 days), 12 (376–427 days), and 20 (610–652 days) months of age, whereas mice of the longitudinal group were allowed to age until they were moribund before euthanization (436–857 days). Criteria for morbidity justifying necropsy of mice in the longitudinal study, approved by The Jackson Laboratory Animal Care and Use Committee, were as follows: not responsive to stimuli, slow respiration, cold to the touch, hunched with matted fur, sudden weight loss, failure to eat and drink, prominent-appearing ribs and spine, and/or sunken hips. Mice were euthanized by CO_2 asphyxiation using methods approved by the American Veterinary Medical Association.

Nine female and 8 male mice entered the study for the 6-month cross-sectional group. Fifteen females and 15 males entered the study for the 12- and 20-month cross-sectional groups. For the longitudinal study, 65 females and 35 males were aged until they became moribund. Not all mice reached the age for the designated group. Thus, a total of 17 mice were necropsied at 6 months of age (9 females and 8 males), 27 mice were necropsied at 12 months of age (15 females and 12 males), 14 mice were necropsied at 20 months of age (7 females and 7 males), and 7 moribund mice were necropsied (4 females and 3 males) (Table 1). Mice found dead were not evaluated due to the rapid onset of autolysis.

The breeding facilities and the mouse rooms were regulated on a 12-hour light/12-hour dark cycle and were maintained at an ambient temperature of 21°C to 23°C. Mice of the same sex (4 per cage) were housed in duplex polycarbonate cages (31 × 31 × 214 cm) on pressurized individually ventilated mouse racks (Thoran Caging System, Hazleton, PA) with a high-efficiency particulate air-filtered supply and exhaust. Mice were allowed ad libitum access to acidified, filtered tap water (pH 2.8–3.2) and pellets containing 6% fat (LabDiet 5K52; PMI Nutritional International, Bentwood, MO). Regular monitoring for viruses, bacteria, parasites, and microsporidium showed that the colonies were free of infestation by any known mouse pathogen (http://jaxmice.jax.org/geneticheath/index.html). All protocols were reviewed and approved by The Jackson Laboratory Animal Care and Use Committee (approval number 06005). Mouse handling and care were followed according to the Public Health Service animal welfare policies.

Tissue Fixation and Preparation

After euthanizing the mice, complete necropsies were performed. [30] Briefly, tissues from all organs (Swiss rolls of the duodenum, jejunum, ileum, and colon [with anus and perineal skin]; longitudinal section of the stomach with esophagus and cecum [inflated with fixative]; cross sections of the left lateral and medial lobes of liver to include the gallbladder, spleen, left and right kidneys with adrenal glands, reproductive organs [testis, epididymis, accessory sex organs, male; ovary, uterine tube, uterus, mammary glands, female], preputial gland for males/clitoral gland for females, salivary gland cluster with cervical lymph nodes, heart, esophagus and trachea with thyroid and parathyroid glands, and tongue; longitudinal sections out of the center of the lobes of both lungs, dorsal skin, ear skin (pinna), ventral skin, muzzle skin, and eyelid; longitudinal section of the hind leg, including the stifle/knee joint; longitudinal section of the front leg, including shoulder and elbow joints; longitudinal section of the hind foot [soft tissues, bone, and nail unit/footpad]; longitudinal section of the

front foot [soft tissues, bone, and nail unit/footpad]; longitudinal section and cross section of the lumbar spine; longitudinal section and cross section of the tail; and sections of the lower jaw; see Table 2) were collected and fixed in Fekete's acid alcohol formalin overnight, after which they were transferred and stored in 70% ethanol. Bones were processed in Cal-Ex (Fisher, Pittsburgh, PA). The cervical spine and skull with brain were collected in Bouin's solution. The skull was cut longitudinally and perpendicularly to provide sections of brain and all bone and soft tissues in the region, including the eye. Pancreata were collected in Bouin's solution and stained with aldehyde fuchsin. Pancreata were also collected and fixed with Fekete's solution with the intestinal rolls. Tissues were then trimmed and embedded in paraffin, cut into 6-mm sections, and stained with hematoxylin and eosin (H&E). Soft tissues with aberrant mineralization were serially sectioned and stained with von Kossa and alizarin red to confirm this process. One set of eyes was removed and fixed in Karnovsky's fixative and processed in plastic[32] from 1 male and 1 female mouse of each strain under investigation. Other cases had the eyes included in the sections of the skull.

Scanning Electron Microscopy

To evaluate the mineralized foci scattered throughout the lungs, scanning electron microscopy (SEM) and element analysis were done by punching out affected areas of lungs in paraffin blocks from one 20-month-old female KK/HlJ and 1 age- and sex-matched C57BL/6J mouse using a skin biopsy punch. Tissues were deparaffinizied, refixed using a paraformaldehyde-glutaraldehyde mix, and postfixed with osmium tetroxide. The samples were critical point dried, mounted on aluminum stubs with double-stick tape, and sputter-coated with a 4-nm layer of gold. They were examined at 20 kV at a working distance of approximately 15 mm on a Hitachi S3000 N VP Scanning Electron Microscope (Hitachi Science Systems, Tokyo, Japan).[2]

Mineralized foci within the KK/HlJ lungs and similar regions from the control lungs were assessed for calcium, magnesium, and phosphorus content by weight using an EDAX x-ray microanalysis system (EDAX, Mahwah, NJ). Samples were examined for an average of at least 300 live seconds to ensure a comprehensive reading was obtained. We use a similar approach to routinely evaluate hair.[22]

Characterization of Lesions

All tissue slides were reviewed by the same experienced, board-certified veterinary pathologist (J.P.S.), except for tissues taken from the central nervous system, which were reviewed by a veterinary neuropathologist (R.T.B.). Physiological phenotyping data, as developed for the International Knockout Mouse Project, [1] were also generated from the same group of KK/HlJ mice. All physiological data are available online through the Mouse Phenome Database (MPD) (http://phenome.jax.org).

Slides were reviewed and diagnoses were entered (and coded) for each individual mouse using the Mouse Disease Information System (MoDIS).[34,36] In MoDIS, anatomical structures (ie, organs) are defined using the Mouse Anatomy Ontology (MA),[11] and histopathological lesions are defined according to the Mouse Pathology Ontology (MPATH).[28] Representative photomicrographs of lesions are available on Pathbase (http://

www.pathbase.net/) and in the Mouse Tumor Biology Database (MTB) (http://www.informatics.jax.org/).[3,17]

Histopathological lesions were quantified by age group and sex as number of lesions per mice and percentage of affected mice.

Blood Electrolytes and Urinalysis

As part of this aging study, blood electrolytes and urinalysis were performed and all data are reported in the MPD. For blood electrolytes, MPD's *Yuan3* data set was used, and for kidney functions, MPD's *Korstanje1* data set for the albumin/creatinine ratio (ACR) was examined.

Results

Number of Mice and Histopathological Lesions per Age Group and Sex

Histopathological lesions in aging KK/HlJ mice were evaluated for each age group and gender. Across all age groups 703 histopathological lesions (409 in females and 294 in males) were observed: 140 in 6-month-old mice (60 in females and 80 in males), 148 in 12-month-old mice (97 in females and 51 in males), 309 in 20-month-old mice (191 in females and 118 in males), and 106 in moribund mice (61 in females and 45 in males) (Tables 1). Thus, an average of 8 (7 for females and 10 for males), 5 (6 for females and 4 for males), 22 (27 for females and 17 for males), and 15 (15 for females and 15 for males) histopathological lesions were observed per mouse in the 6-month, 12-month, 20-month, and longitudinal mouse groups, respectively (Table 1).

Histopathological Lesions

Detailed information about the quantity of histopathological lesions is presented in Table 2. Aberrant mineralization was the most frequently observed lesion (1.8 lesions/mouse) (Figs. 1, 2) and was found in several tissues, particularly in the vibrissa dermal sheath (Fig. 4), heart (Figs. 5, 6), lung (Figs. 7–9), testis, and blood vessels (Fig. 10), but also in kidney, skeletal muscles, ear, eye (Fig. 11), spleen, ovary, fat, and brain. Representative serial sections were stained with von Kossa and alizarin red to verify that changes interpreted to be mineralization in H&E-stained slides were actually mineralized. Electron microscopic examination of the lung revealed that mineralization is primarily located within the alveolar walls (Figs. 8, 9). Aberrant mineralization was most common in mice 20 months old and older (Fig. 3).

Besides mineralization, hyperplasia was another commonly observed histopathological lesion (1.7 lesions/mouse) and was found primarily in pancreatic islets (Figs. 12, 13). Similar to mineralization, the number of mice with hyperplasia was the highest at 20 months but was less frequent in mice of the longitudinal study group (Fig. 14). Detailed numbers for hyperplasias at all ages are listed in the Table 2.

Another distinct pathological lesion in KK/HlJ mice included fibro-osseous lesions (0.5 diagnoses/female mouse).

Affected Organs

Organs with frequent histopathological lesions are presented in Figure 15. Lesions were most common in pancreata (1.8 lesions/mouse) and kidneys (0.9 lesions/mouse). Although lesions in pancreata were primarily hyperplasia of pancreatic islets (Fig. 16), those lesions in kidneys were mostly membranous glomerulonephritis and chronic interstitial nephritis (Fig. 17). Besides pancreata and kidneys, 55 other organs also had lesions. In 20 organs (ie, heart, preputial gland, vibrissa dermal sheath, thyroid gland, clitoral gland, skin, lung, testis, bone, teeth, ovary, skeletal muscle, uterus, spleen, nasal cavity, liver, eye, stomach, adrenal gland, and the ear), a total of 10 or more lesions were found (ie, 0.15 or more lesions/mouse) (Fig. 15). Numbers of histopathological lesions for each organ at all time points are reported in Table 2.

Blood Electrolytes and Urinalysis

Ranges of blood electrolytes and the ACR among all strains of the aging study and, for comparison, for KK/HlJ are reported in Table 3. KK/HlJ mice had the lowest blood calcium concentration of all strains at 12 and 20 months of age, the lowest magnesium concentration at 20 months of age, and the highest blood iron concentration of all strains at 6 months of age. All other electrolytes were within the range of all investigated strains. The ACR was highest among all strains both at 12 and 20 months. No data for urinalysis are available for the 6-month group (Table 3).

Discussion

A comprehensive evaluation of histopathological lesions in aging mice of the inbred strain KK/HlJ is provided. Many lesions found in old KK/HlJ mice are similar to those found in most inbred strains that are described and illustrated in standard mouse pathology textbooks.[8,23,24] Most commonly, lesions were observed in pancreata and kidneys. Lesions in the pancreata were primarily due to hyperplasia of the pancreatic islets. Although this is a common, nonspecific change observed in aging,[27] KK/HlJ has previously been recognized for its susceptibility to T2D due to inherited glucose intolerance and insulin resistance,[14] suggesting that the histopathological changes in the pancreata may be functional.

The kidneys were the second most commonly affected organs, frequently diagnosed with membranous glomerulonephritis and chronic interstitial nephritis. Those kidney changes are common findings in older mice of many strains.[35] In KK/HlJ mice, these changes seem to be functional, as indicated by the elevated plasma albumin-to-creatinine ratios compared with all other strains at 12 and 20 months of age. In addition, diabetic nephropathy previously has been reported to be secondary to hyperglycemia,[10] which is a characteristic of KK/HlJ mice.

In a previous publication, it was mentioned that there are aging-related vascular mineralizations of the heart and kidney in KK/HlJ mice.[18] The current study also identified aberrant mineralization in the vasculature as well as in several other tissues. Most frequently, mineralization foci were found in the vibrissa dermal sheath, heart, and lung. Currently, the details on genetic and environmental risk factors leading to these

mineralization events are unclear, but investigations to unravel the genetic basis of mineralization in KK/HlJ mice are under way. Recent reports have suggested the role of a polymorphism in the mouse adenosine triphosphate binding cassette, subfamily C (CFTR/MRP), member 6 (*Abcc6*) gene,[5,20] which encodes an efflux transporter protein, ABCC6, expressed primarily in the liver and, to a lesser extent, in the kidneys. This gene has been associated with aberrant mineralization in soft connective tissues in skin, eye, and the cardiovascular system in humans with PXE, an autosomal recessive disorder. *Abcc6* knockout mice (eg, *Abcc6*^{tm1JfK} and *Abcc6*^{tm1Aabb}) recapitulate the genetic, histopathologic, and ultrastructural features of PXE.[9,16] Aberrant mineralization was confirmed using von Kossa and alizarin red stains (data not shown) and element analysis as previously published.[5,20] As *Abcc6*^{tm1JfK} and KK/HlJ mice show comparable traits, KK/HlJ has recently been proposed as a novel mouse model for PXE.[5,20]

Besides genetic risk factors, environmental conditions could potentially contribute to systemic mineralization. Aberrant mineralization in KK/HlJ mice is unlikely due to dietary imbalance of minerals or vitamins because of the controlled environmental conditions. In fact, the 31 strains of the aging strain survey were maintained under the same environment, and no other strain was found to have systemic mineralization to the level found in the KK/HlJ strain.[5] Kavukcuoglu et al[15] demonstrated that the aberrant mineralization foci in *Abcc6*^{tm1Jfk} mice consist of calcium hydroxyapatite with calcium and phosphorus as the principal ions. It is unlikely that the deposits consisting of calcium and phosphate are due to increased calcium intake, as evidenced by decreased calcium and normal phosphate serum concentrations in KK/HlJ mice, and, particularly, in light of a previous report that showed that KK/HlJ mice consistently avoided intake of calcium-enriched solutions.[37] Finally, water, available ad libitum, was obtained from local lakes in an area consisting of granite (Bar Harbor, ME), such that dissolved minerals, primarily calcium, would not be high.

KK/HlJ was recently described as the most responsive strain for naive airway hyperresponsiveness among 36 inbred strains of mice.[4,19] This observation was surprising because traditionally, A/J mice were used as the hyperresponsive model in genetic studies of asthma phenotypes.[6,7,38] Here, our histopathological analysis revealed mineralization processes in the lung, particularly in the alveolar walls. It remains to be investigated if the mineralization in the lung could potentially lead to obstruction of the surrounding airways or if the mineralization and aberrant airway functions are separate pathological entities. The latter may be more likely due to the fact that mineralization in the lungs was more frequent in older mice, but investigations on airway hyperresponsiveness were commonly conducted in young adults (8–12 weeks old).

In summary, a comprehensive, detailed histopathologic analysis of aging mice of the strain KK/HlJ is provided here. The outstanding characteristic of this strain is the systemic aberrant mineralization across multiple organs. Although mineralization of the vasculature was reported in the past, mineralization in other tissues such as the lung or vibrissae dermal sheaths is a novel observation, which is potentially related to functional characteristics of this particular strain. In addition to evidence of mineralization, this study provides detailed information about histopathological lesions in KK/HlJ mice as they age that can help investigators choose the right mouse model and appropriately interpret research data.

Acknowledgements

We thank Jesse Hammer for his technical assistance in preparing the figures.

Funding

The author(s) disclosed receipt of the following financial support for the research, authorship and/or publication of this article: This work was supported by grants from the Ellison Medical Foundation and the National Institutes of Health (AG25707 for the Shock Aging Center). Dr Berndt is the recipient of a fellowship by the Parker B. Francis Foundation, and Dr Li is recipient of a Dermatology Foundation Research Career Development Award. Drs Berndt and Li are recipients of North American Hair Research Society Mentorship Grants. The Jackson Laboratory Shared Scientific Services were supported in part by a Basic Cancer Center core grant from the National Cancer Institute (CA34196).

References

1. Austin CP, Battey JF, Bradley A, et al. The knockout mouse project. Nat Genet. 2004; 36:921–924. [PubMed: 15340423]
2. Bechtold, LS. Ultrastructural evaluation of mouse mutations. In: Sundberg, JP.; Boggess, D., editors. Systematic Characterization of Mouse Mutations. Boca Raton, FL: CRC Press; 2000. p. 121-129.
3. Begley DA, Krupke DM, Neuhauser SB, et al. The Mouse Tumor Biology Database (MTB): a central electronic resource for locating and integrating mouse tumor pathology data. Vet Pathol. 2012; 49:218–223. [PubMed: 21282667]
4. Berndt A, Leme AS, Williams LK, et al. Comparison of unrestrained plethysmography and forced oscillation for identifying genetic variability of airway responsiveness in inbred mice. Physiol Genomics. 2011; 43:1–11. [PubMed: 20823217]
5. Berndt A, Li Q, Potter CS, et al. A single-nucleotide polymorphism in the *Abcc6* gene associates with connective tissue mineralization in mice similar to targeted models for pseudoxanthoma elasticum. J Invest Dermatol. 2013; 133:833–836. [PubMed: 23014343]
6. Ewart SL, Kuperman D, Schadt E, et al. Quantitative trait loci controlling allergen-induced airway hyperresponsiveness in inbred mice. Am J Respir Cell Mol Biol. 2000; 23:537–545. [PubMed: 11017920]
7. Ewart SL, Mitzner W, DiSilvestre DA, et al. Airway hyperresponsiveness to acetylcholine: segregation analysis and evidence for linkage to murine chromosome 6. Am J Respir Cell Mol Biol. 1996; 14:487–495. [PubMed: 8624254]
8. Frith, CH.; Ward, JM. Color Alas of Neoplastic and Non-Neoplastic Lesions in Aging Mice. Amsterdam: Elsevier; 1988.
9. Gorgels TG, Hu X, Scheffer GL, et al. Disruption of *Abcc6* in the mouse: novel insight in the pathogenesis of pseudoxanthoma elasticum. Hum Mol Genet. 2005; 14:1763–1773. [PubMed: 15888484]
10. Han BG, Hao CM, Tchekneva EE, et al. Markers of glycemic control in the mouse: comparisons of 6-h- and overnight-fasted blood glucoses to Hb A1c. Am J Physiol Endocrinol Metab. 2008; 295:E981–E986. [PubMed: 18664598]
11. Hayamizu TF, Mangan M, Corradi JP, et al. The Adult Mouse Anatomical Dictionary: a tool for annotating and integrating data. Genome Biol. 2005; 6:R29. [PubMed: 15774030]
12. Herberg L, Coleman DL. Laboratory animals exhibiting obesity and diabetes syndromes. Metabolism. 1977; 26:59–99. [PubMed: 834144]
13. Huang LH, Sery TW. Corneal degeneration in a congenitally diabetic inbred strain of mouse. Br J Ophthalmol. 1971; 55:266–271. [PubMed: 5313900]
14. Ikeda H. KK mouse. Diabetes Res Clin Pract. 1994; 24(suppl):S313–S316. [PubMed: 7859626]
15. Kavukcuoglu NB, Li Q, Pleshko N, et al. Connective tissue mineralization in *Abcc6*$^{-/-}$ mice, a model for pseudoxanthoma elasticum. Matrix Biol. 2012; 31:246–252. [PubMed: 22421595]
16. Klement JF, Matsuzaki Y, Jiang QJ, et al. Targeted ablation of the *Abcc6* gene results in ectopic mineralization of connective tissues. Mol Cell Biol. 2005; 25:8299–8310. [PubMed: 16135817]

17. Krupke DM, Begley DA, Sundberg JP, et al. The Mouse Tumor Biology database. Nat Rev Cancer. 2008; 8:459–465. [PubMed: 18432250]
18. Leiter EH. Selecting the “right” mousemodel formetabolic syndrome and type 2 diabetes research. Methods Mol Biol. 2009; 560:1–17. [PubMed: 19504239]
19. Leme AS, Berndt A, Williams LK, et al. A survey of airway responsiveness in 36 inbred mouse strains facilitates gene mapping studies and identification of quantitative trait loci. Mol Genet Genomics. 2010; 283:317–326. [PubMed: 20143096]
20. Li Q, Berndt A, Guo H, et al. A novel animal model for pseudoxanthoma elasticum: the KK/HlJ mouse. Am J Pathol. 2012; 181:1190–1196. [PubMed: 22846719]
21. Lu G, Uga S, Miyata M, et al. Histopathological study of congenitally diabetic yellow KK mouse lens. Jpn J Ophthalmol. 1993; 37:369–378. [PubMed: 8145381]
22. Mecklenburg L, Paus R, Halata Z, et al. FOXN1 is critical for onycholemmal terminal differentiation in nude (*Foxn1*) mice. J Invest Dermatol. 2004; 123:1001–1011. [PubMed: 15610506]
23. Mohr, U.; Dungworth, DL.; Capen, CC., et al. Pathobiology of the Aging Mouse. Vol. Vol 2. Washington, DC: ILSI Press; 1996.
24. Mohr, U.; Dungworth, DL.; Capen, CC., et al. Pathobiology of the Aging Mouse. Vol. Vol 1. Washington, DC: ILSI Press; 1996.
25. Qi Z, Fujita H, Jin J, et al. Characterization of susceptibility of inbred mouse strains to diabetic nephropathy. Diabetes. 2005; 54:2628–2637. [PubMed: 16123351]
26. Reddi AS, Velasco CA, Reddy PR, et al. Diabetic microangiopathy in KK mice, VI: effect of glycemic control on renal glycoprotein metabolism and established glomerulosclerosis. Exp Mol Pathol. 1990; 53:140–151. [PubMed: 2148155]
27. Sass B, Vernon ML, Peters RL, et al. Mammary tumors, hepato-cellular carcinomas, and pancreatic islet changes in C3H-Avy Mice. J Natl Cancer Inst. 1978; 60:611–621. [PubMed: 203711]
28. Schofield PN, Sundberg JP, Sundberg BA, et al. The mouse pathology ontology, MPATH: structure and applications. J Biomed Semantics. In press.
29. Shimada T. Correlation between metabolic and histopathological changes in the myocardium of the KK mouse: effect of diltiazem on the diabetic heart. Jpn Heart J. 1993; 34:617–626. [PubMed: 8301847]
30. Silva, KA.; Sundberg, JP. Necropsy methods. In: Hedrich, HJ., editor. The Laboratory Mouse. London: Academic Press; 2012.
31. Silver, LM. Mouse Genetics: Concepts and Applications. New York: Oxford University Press; 1995.
32. Smith, RS.; John, SWM.; Nashina, PM., et al. Systematic Evaluation of the Mouse Eye: Anatomy, Pathology, and Biomethods. Boca Raton, FL: CRC Press; 2002.
33. Staats J. Standardized nomenclature for inbred strains of mice: fifth listing. Cancer Res. 1972; 32:1609–1646. [PubMed: 5044129]
34. Sundberg BA, Schofield PN, Gruenberger M, et al. A data-capture tool for mouse pathology phenotyping. Vet Pathol. 2009; 46:1230–1240. [PubMed: 19605915]
35. Sundberg JP, Benrdt A, Sundberg BA, et al. The mouse as a model for understanding chronic diseases of aging: the histopathologic basis of aging in inbred mice [published online June 1, 2011]. Pathobiol Aging Age Relat Dis.
36. Sundberg JP, Sundberg BA, Schofield P. Integrating mouse anatomy and pathology ontologies into a phenotyping database: tools for data capture and training. Mamm Genome. 2008; 19:413–419. [PubMed: 18797968]
37. Tordoff MG, Bachmanov AA, Reed DR. Forty mouse strain survey of voluntary calcium intake, blood calcium, and bone mineral content. Physiol Behav. 2007; 91:632–643. [PubMed: 17493644]
38. Wills-Karp M, Ewart SL. The genetics of allergen-induced airway hyperresponsiveness in mice. Am J Respir Crit Care Med. 1997; 156:S89–S96. [PubMed: 9351586]
39. Zheng QY, Johnson KR, Erway LC. Assessment of hearing in 80 inbred strains of mice by ABR threshold analyses. Hear Res. 1999; 130:94–107. [PubMed: 10320101]

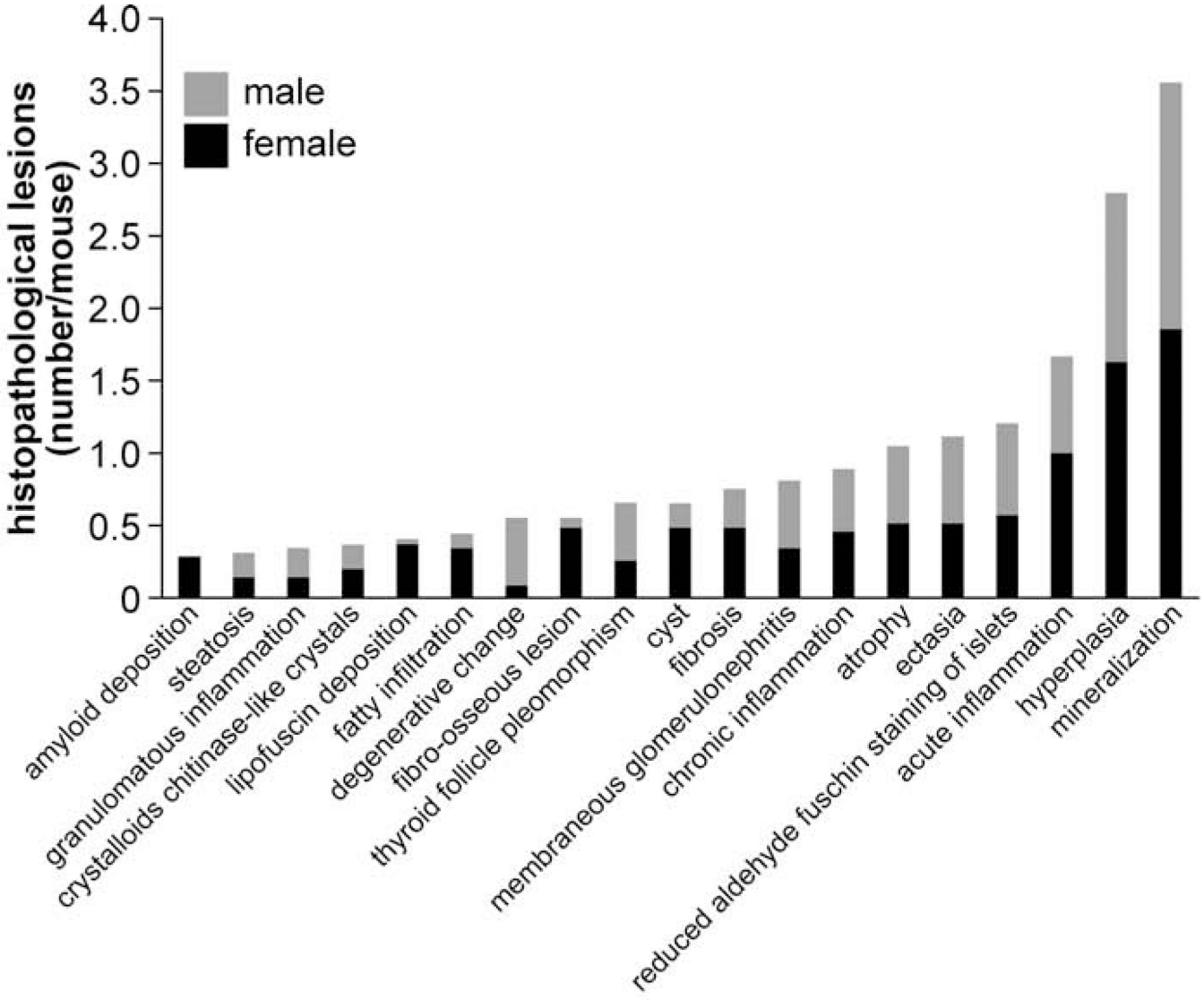

Figure 1.

Type and frequency of histopathological lesions across all organs. Bars show the additive number of processes for female (black) and male (gray) mice.

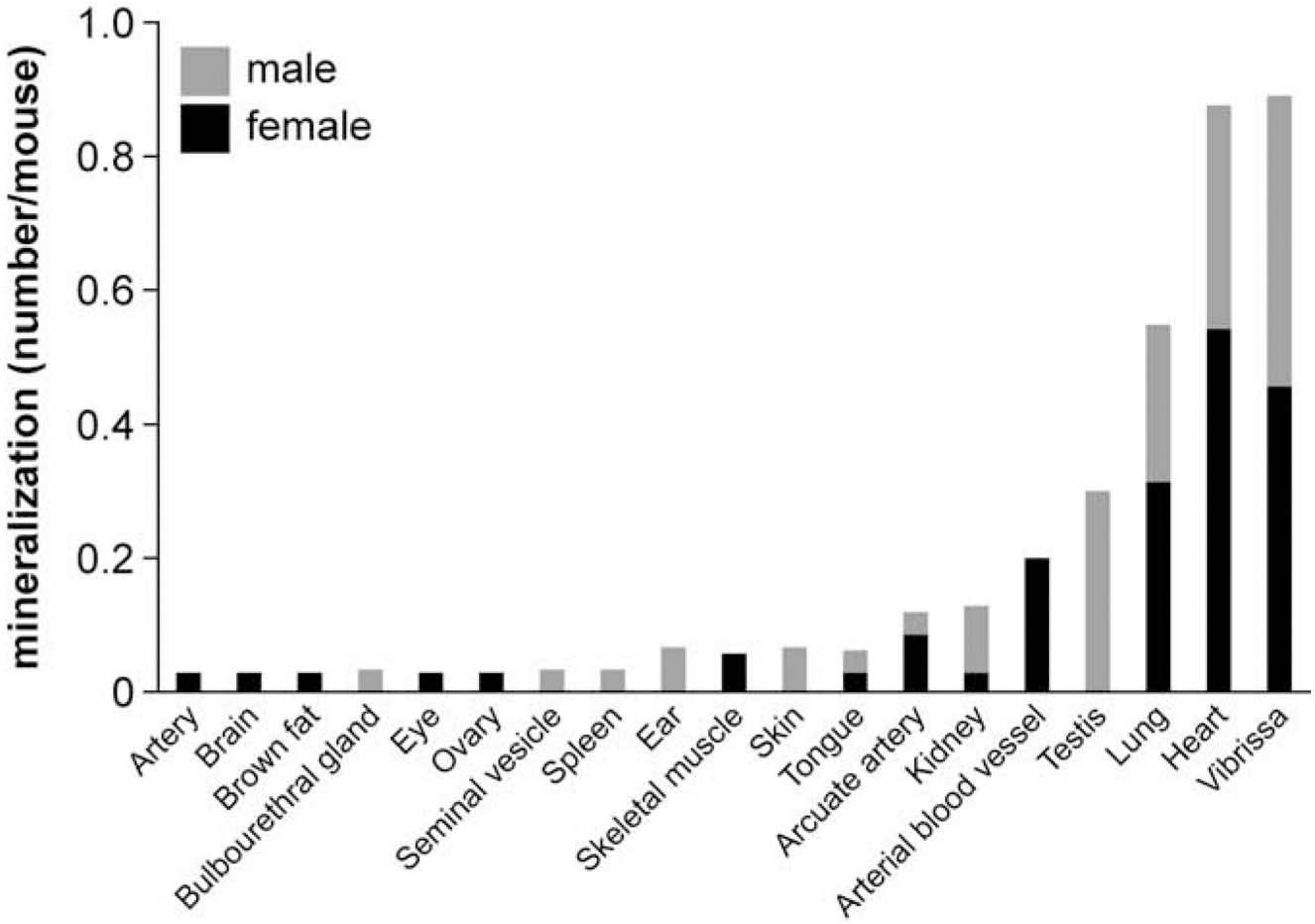

Figure 2.

Frequency of mineralization lesions in different organs. Bars show the additive number of lesions for female (black) and male (gray) mice.

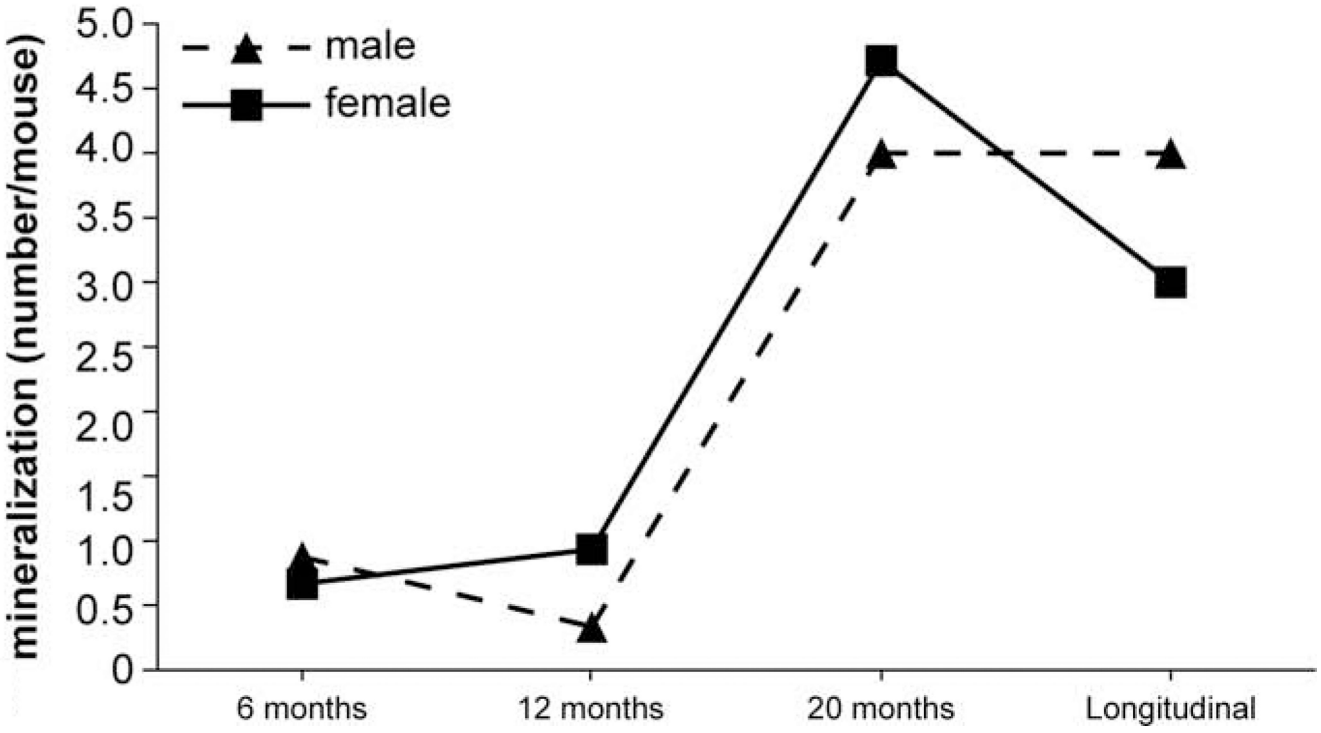

Figure 3.
Frequency of mineralization lesions at different ages. The solid line represents females and dashed line represents males.

Figure 4.
Muzzle skin, vibrissa; 624-day-old female KK/HlJ mouse, case No. 1. There is mineralization of the connective tissue sheath of vibrissae (arrows). Hematoxylin and eosin (HE).

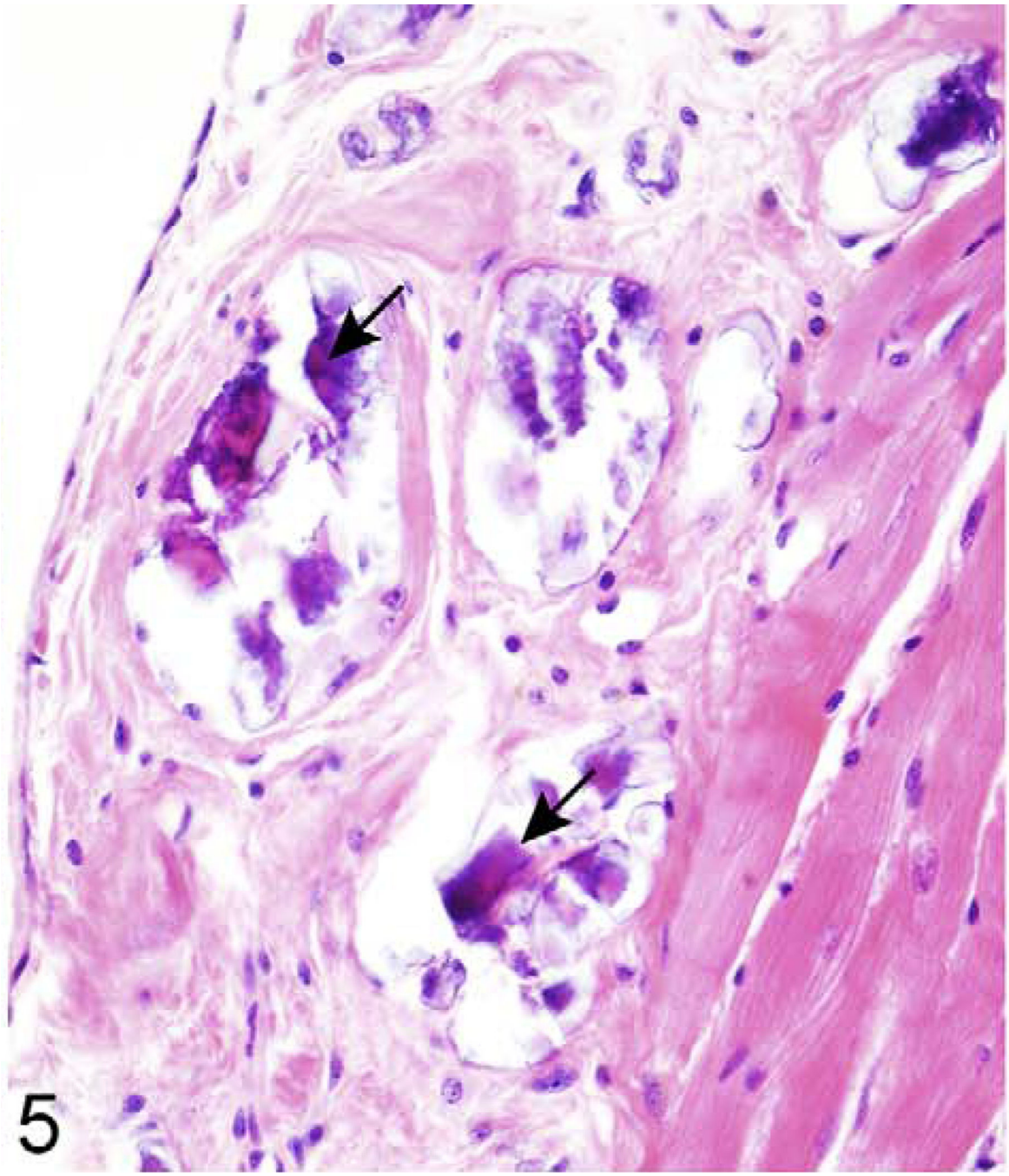

Figure 5.
Right ventricle, epicardium; 624-day-old female KK/HlJ mouse, case No. 2. Epicardial fibrosis and mineralization (arrows) are a prominent feature in the right ventricular free wall of the heart. HE.

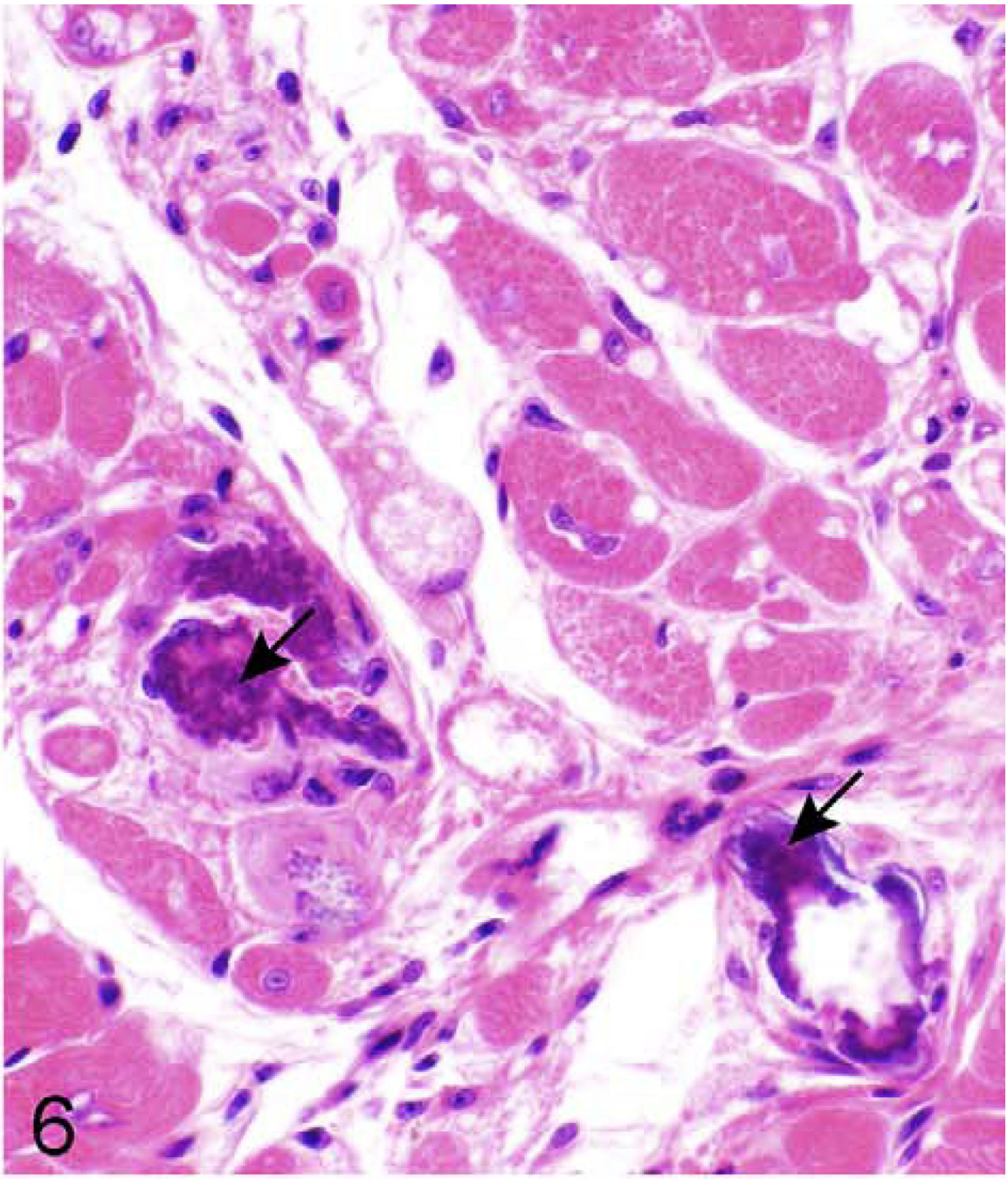

Figure 6.
Myocardium, left ventricle; 624-day old-KK/HlJ female mouse, case No. 2. Mineralization (arrows) with minimal fibrosis is evident in the heart. HE.

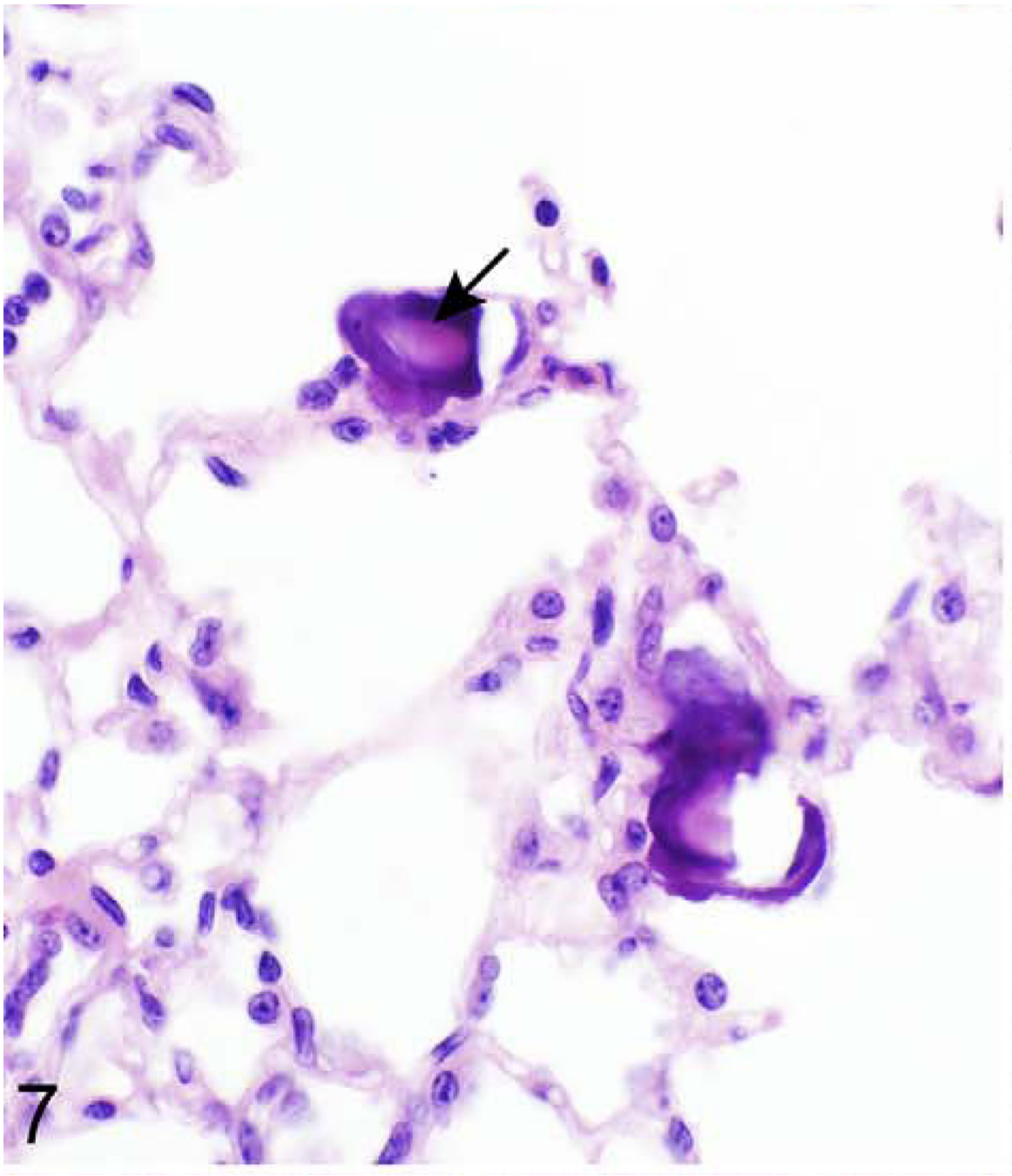

Figure 7.
Lung; 624-dayold female KK/HlJ mouse, case No. 2. Multiple foci of mineralization are present within the alveolar septa (arrow). HE.

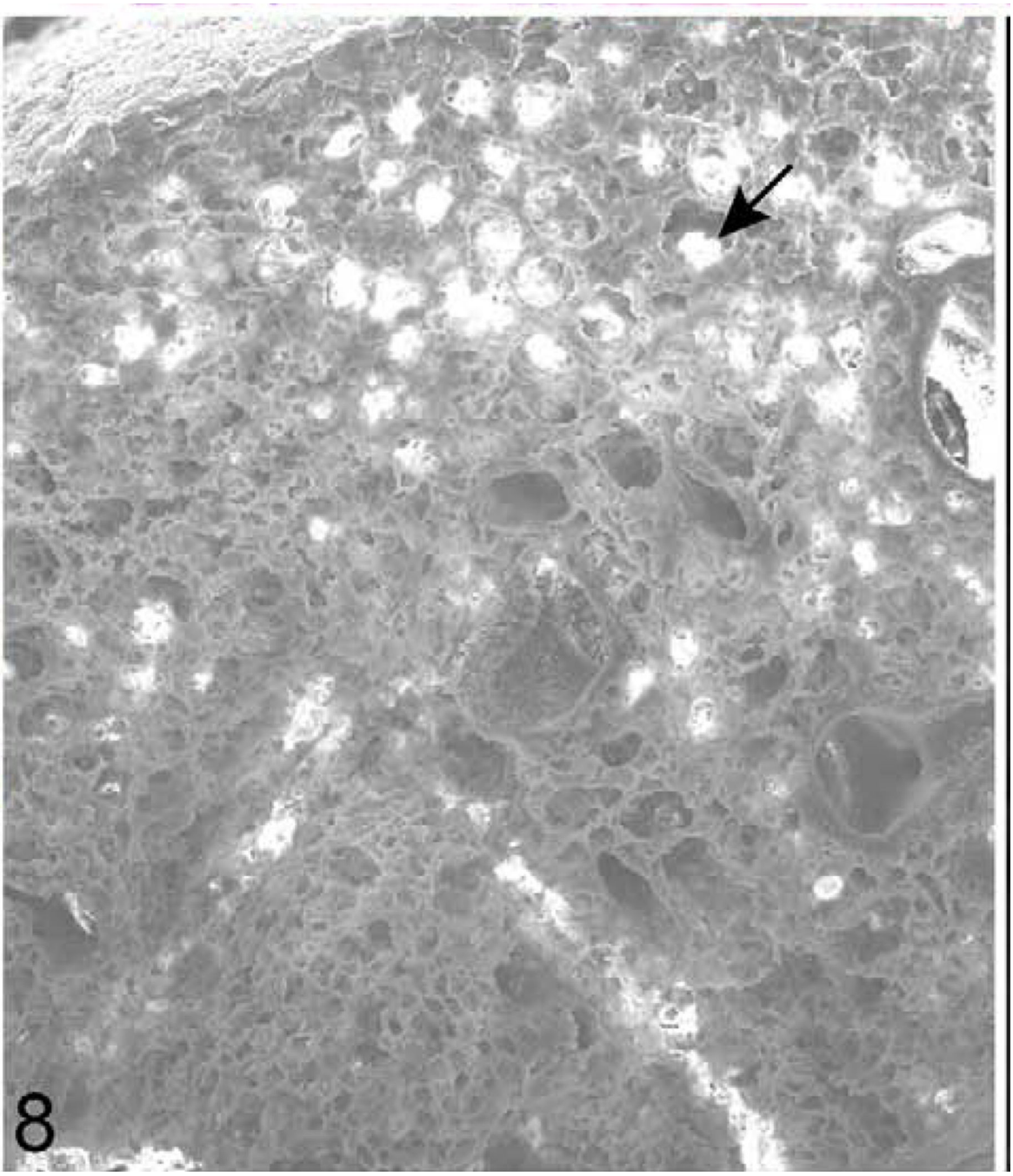

Figure 8.
Lung; 624-day-old female KK/HlJ mouse; case No. 2. Horizontal plane of lung illustrating mineralization foci in the alveoli (arrow). Gold sputter coat, scanning electron microscopy (SEM).

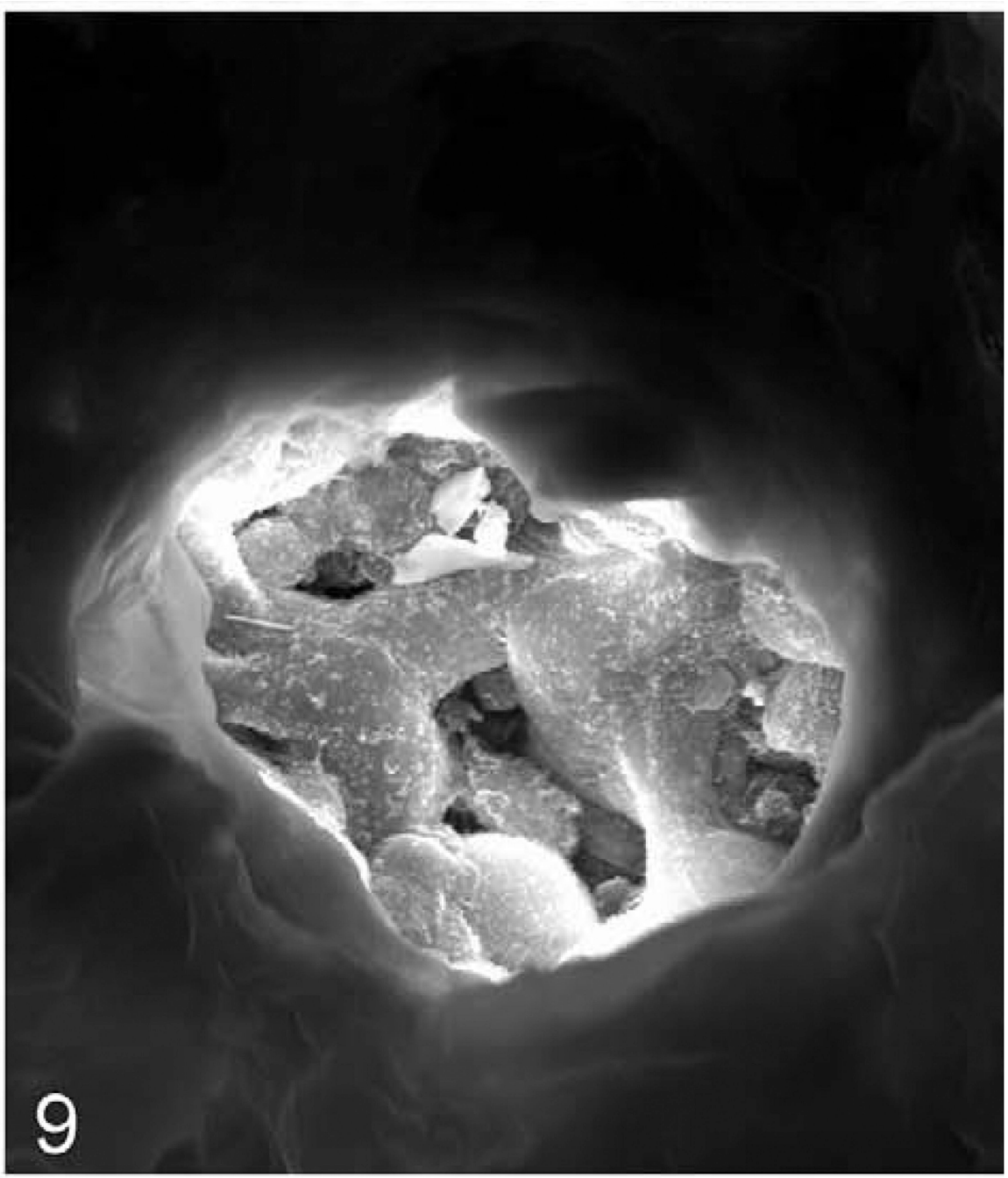

Figure 9.
Lung; 624-day-old female KK/HlJ mouse, case No. 2. Higher magnification of focus marked with an arrow in Figure 8 to illustrate the mineralization. Gold sputter coat, SEM.

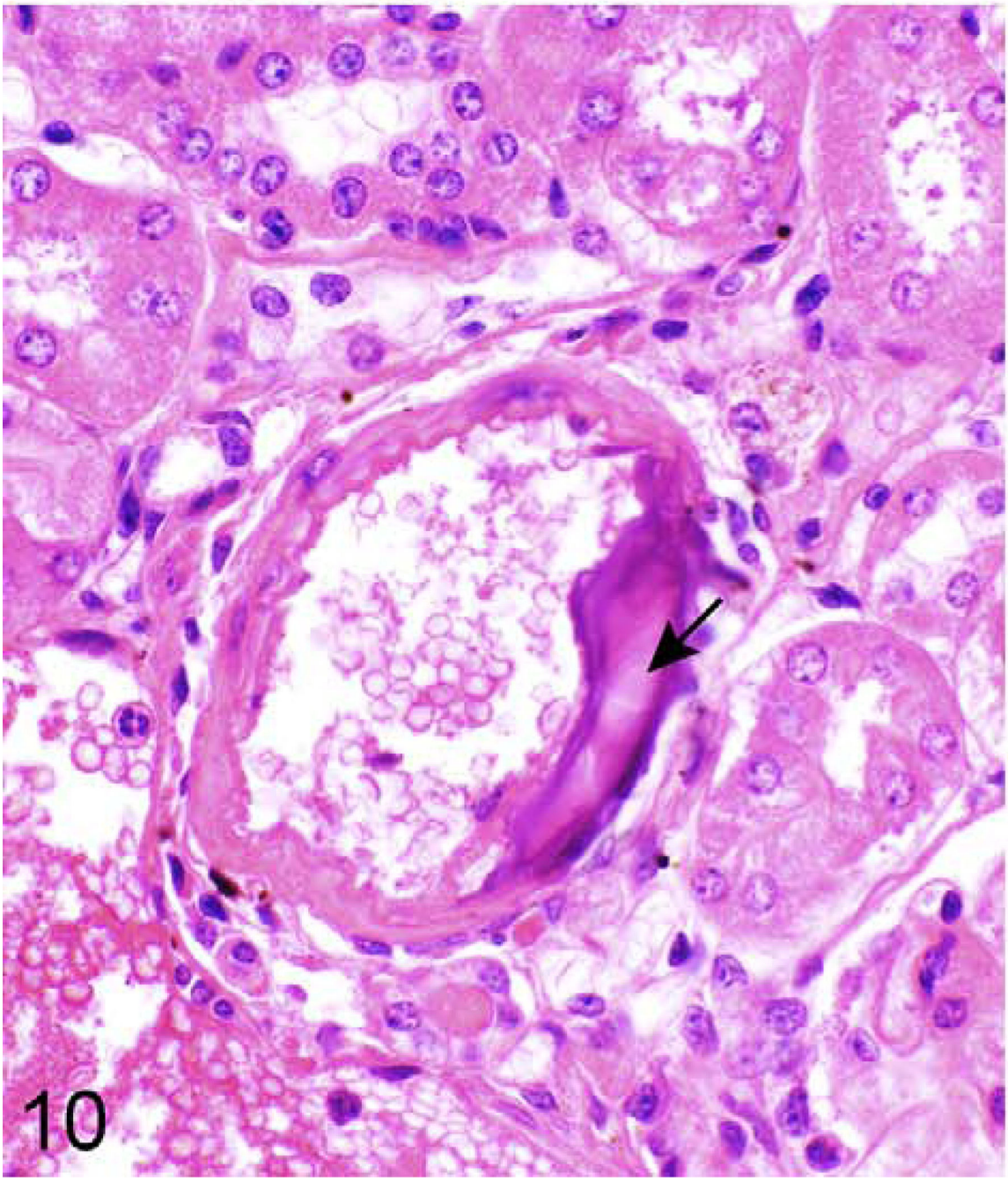

Figure 10.
Kidney (arcuate artery); 624-day-old female KK/HlJ mouse, case No. 3. Mineralization (arrow) of the arterial wall. HE.

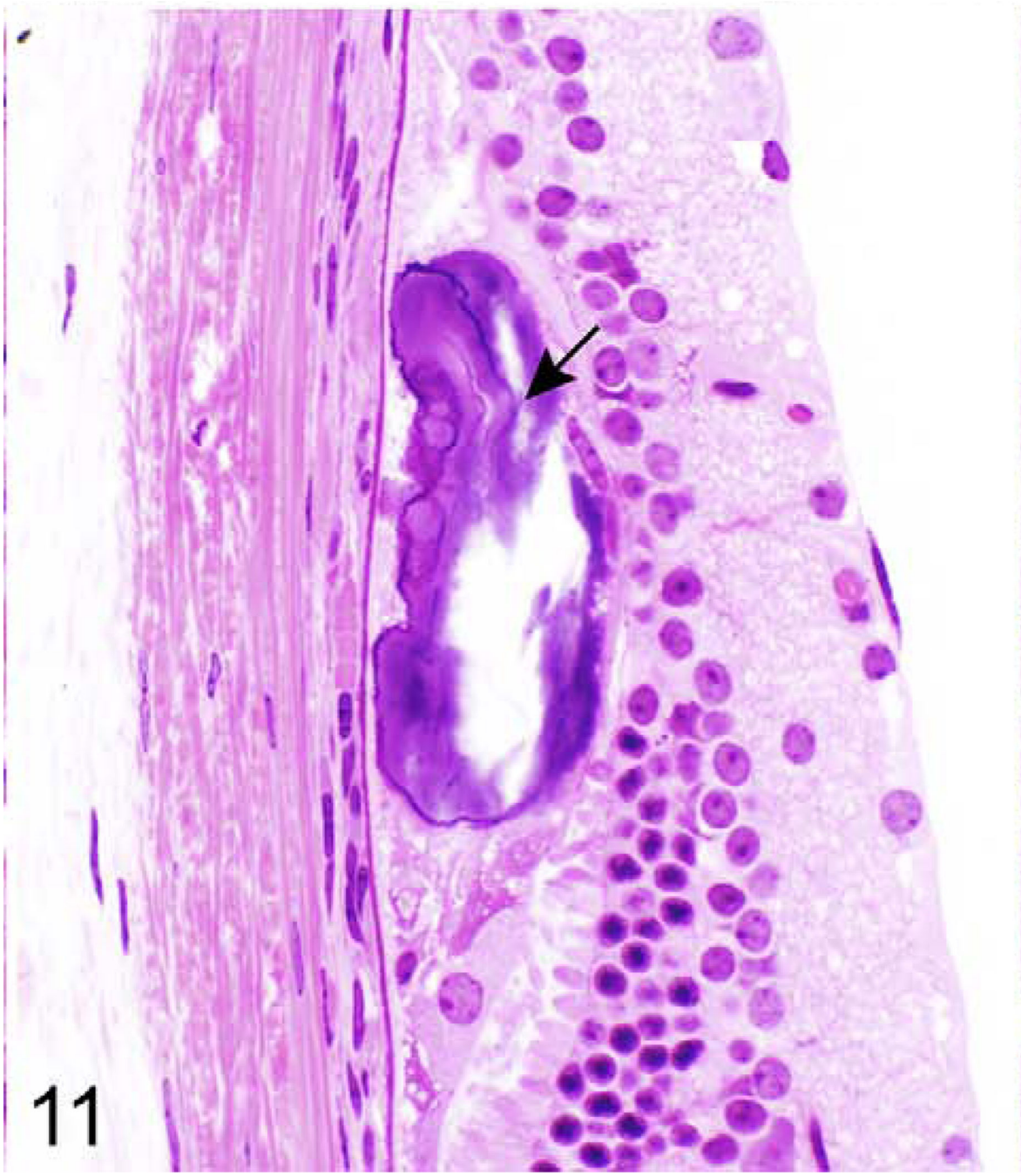

Figure 11.
Retina; 624-day-old female KK/HlJ mouse, case No. 4. Mineralization (arrow) at the base of the retina. HE.

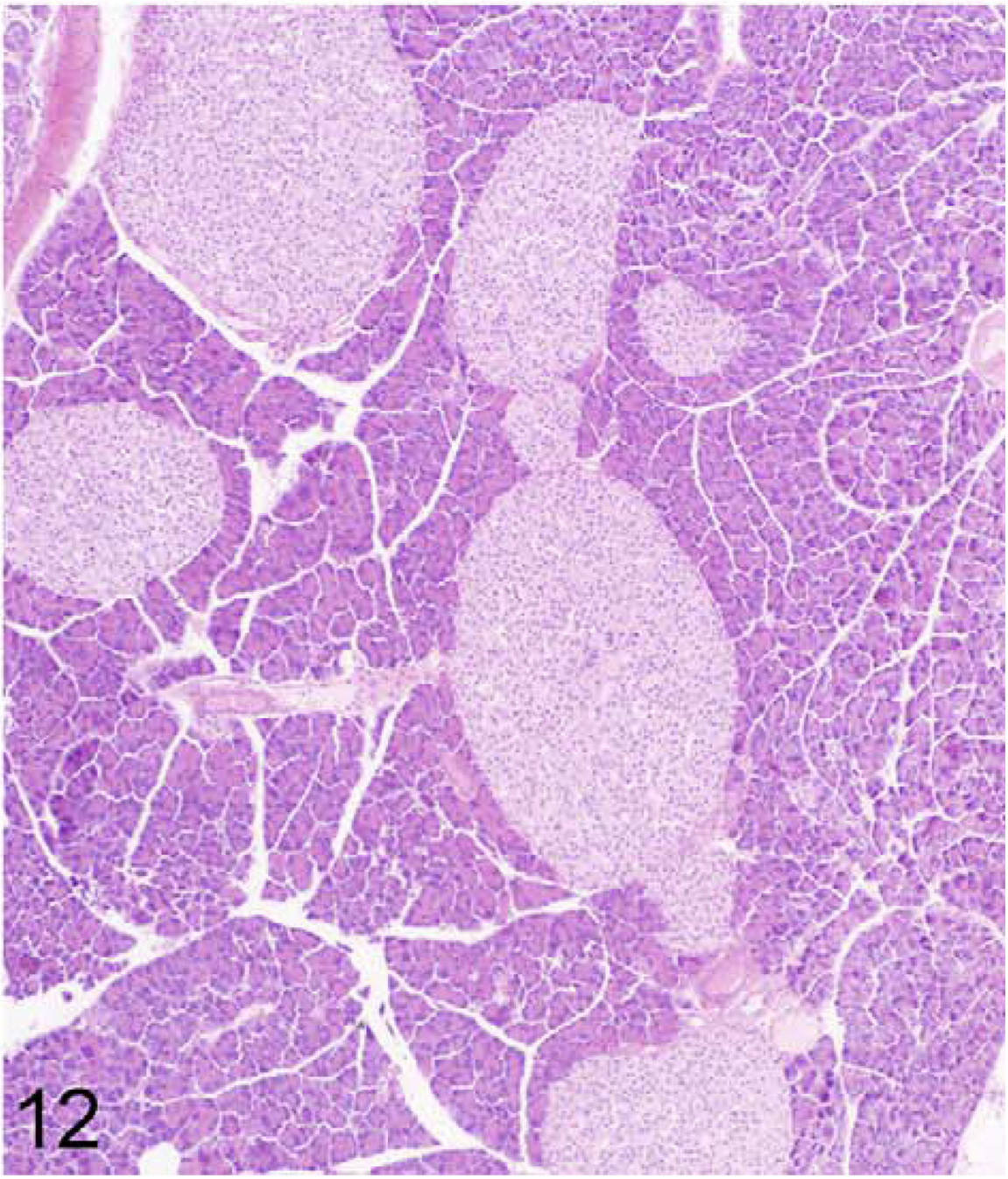

Figure 12.
Pancreas; 384-day-old male KK/HlJ mouse, case No. 5. A severe case of pancreatic islet hyperplasia. HE.

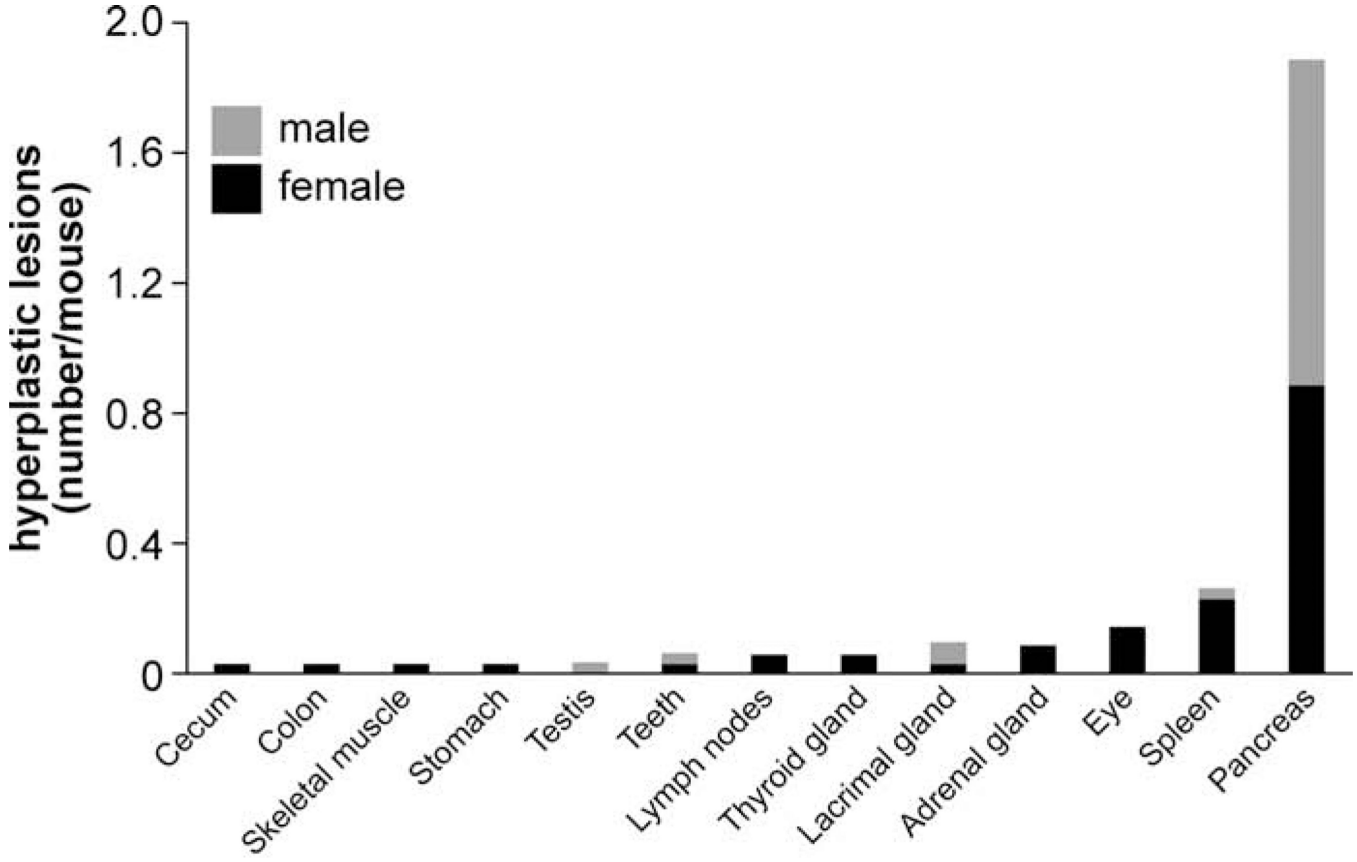

Figure 13.
Frequency of hyperplasia across several organs. The bars show the additive number of processes for female (black) and male (gray) mice.

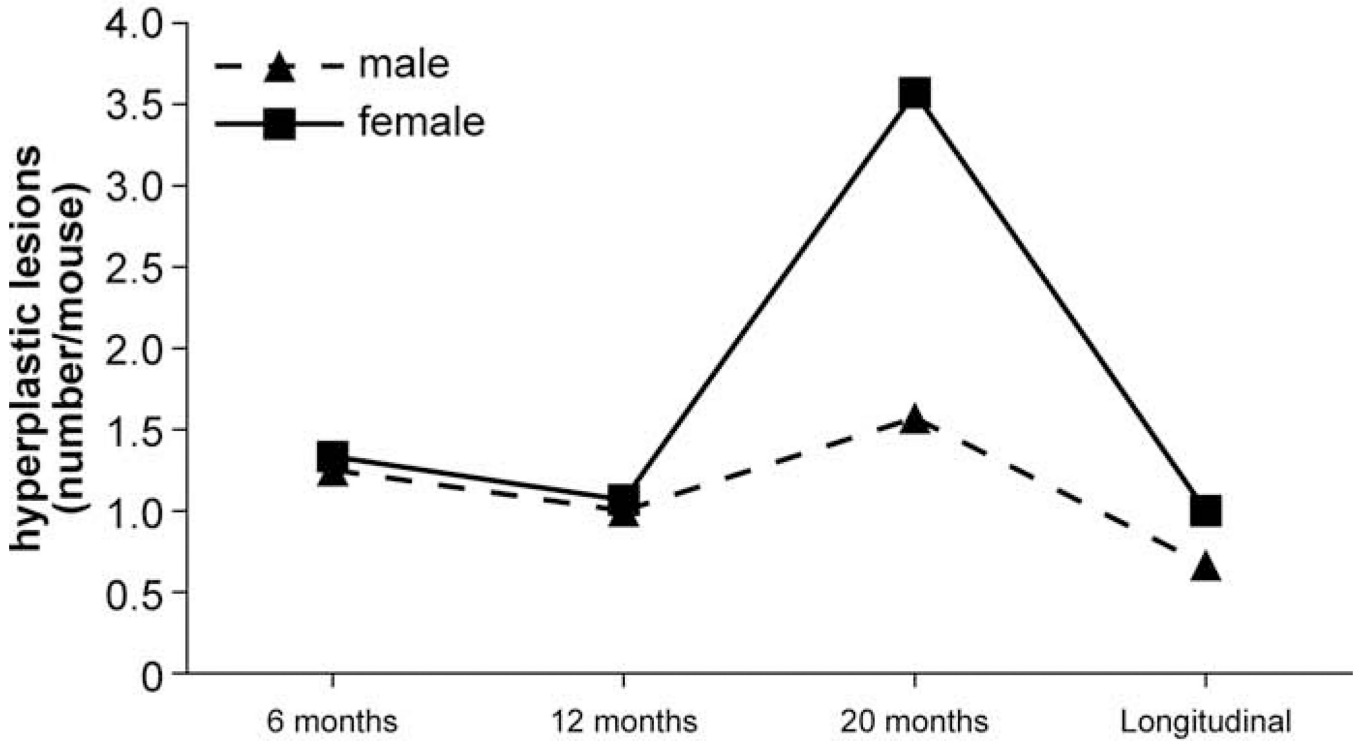

Figure 14.
Frequency of hyperplasia across all organs at different ages. The solid line represents females and dashed line represents males.

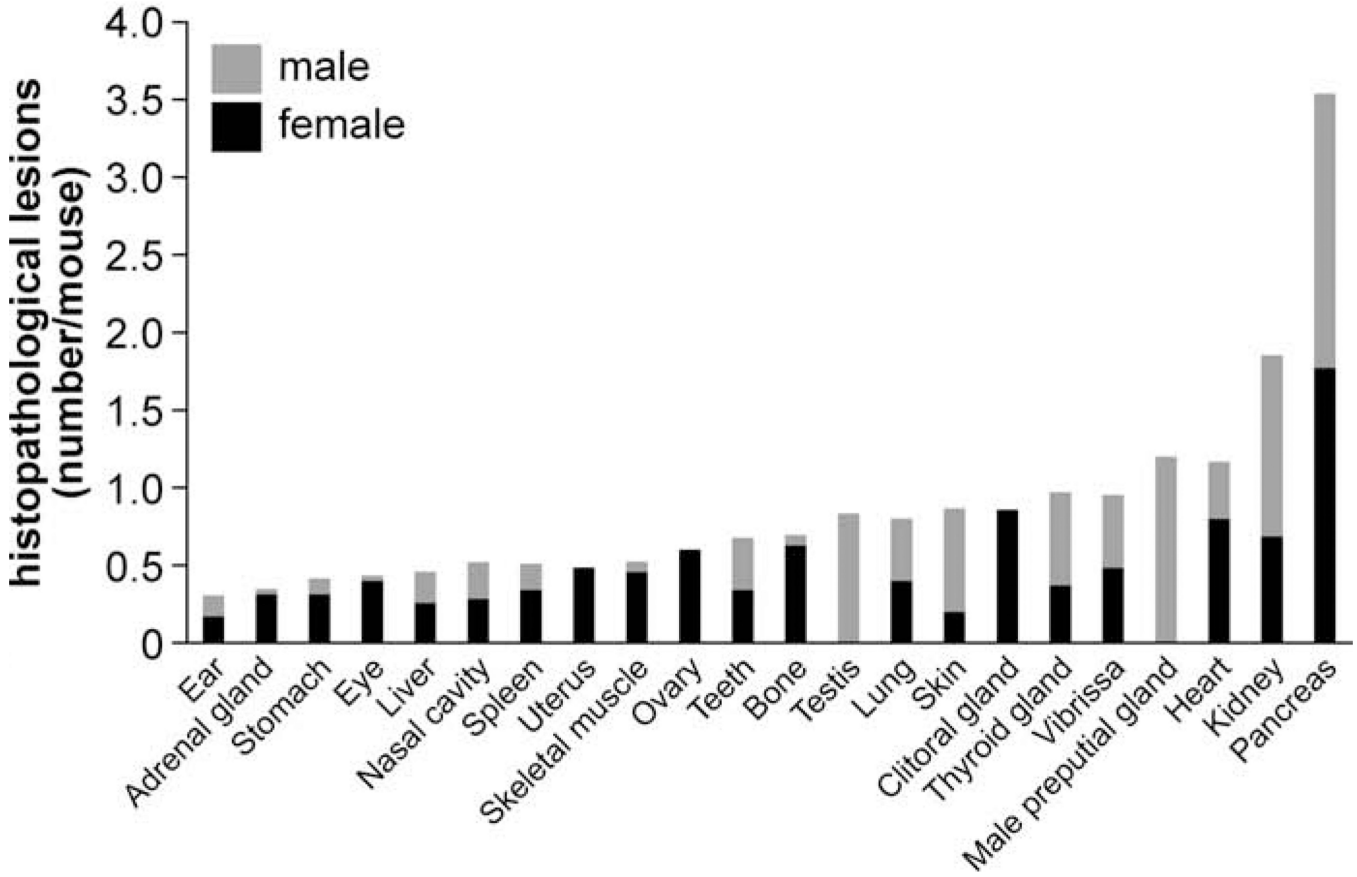

Figure 15.

Frequency of histopathological lesions in different organs. Bars show the additive number of processes for female (black) and male (gray) mice.

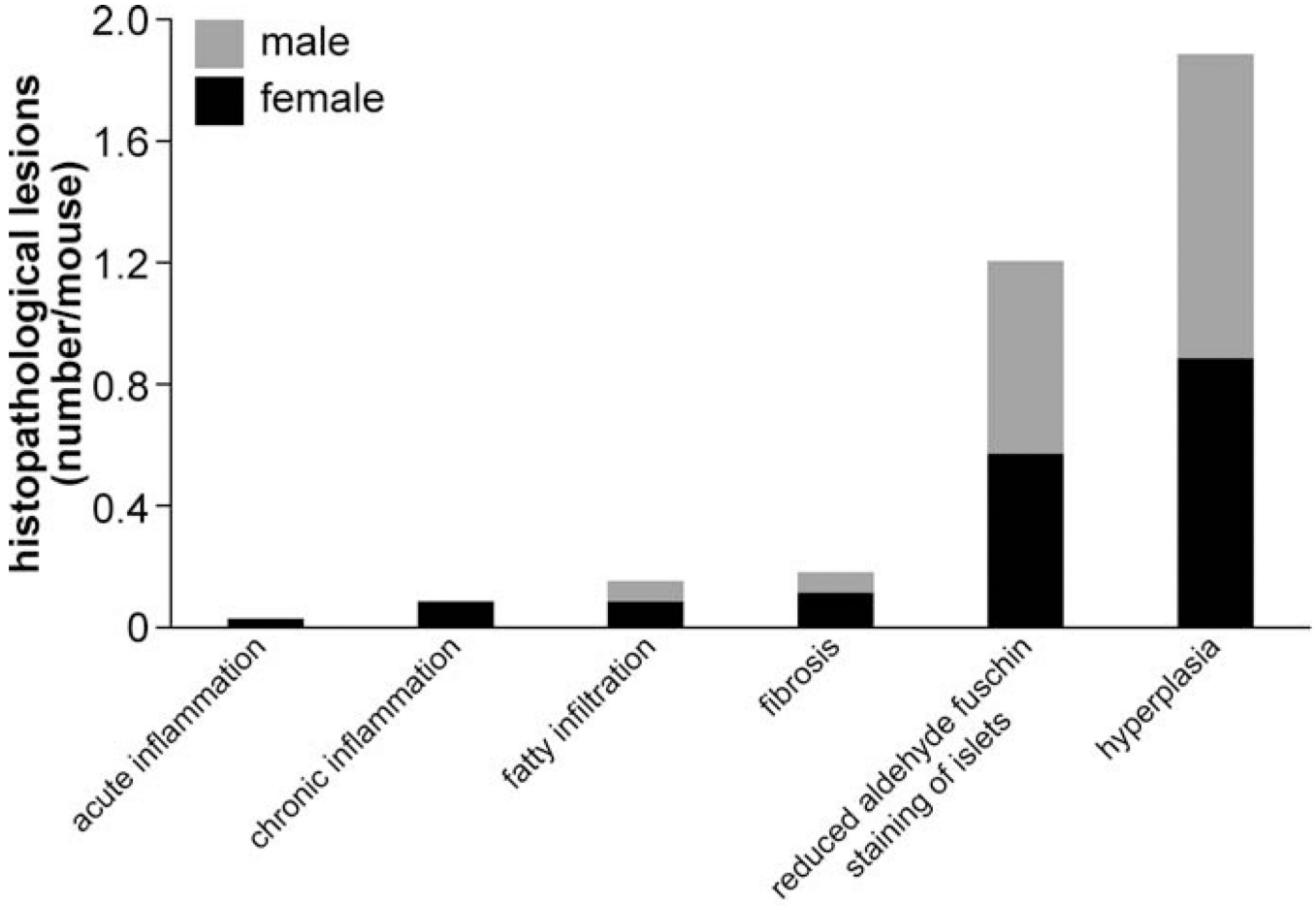

Figure 16.

Frequency of histopathological lesions in pancreata. Bars show the additive number of lesions for female (black) and male (gray) mice.

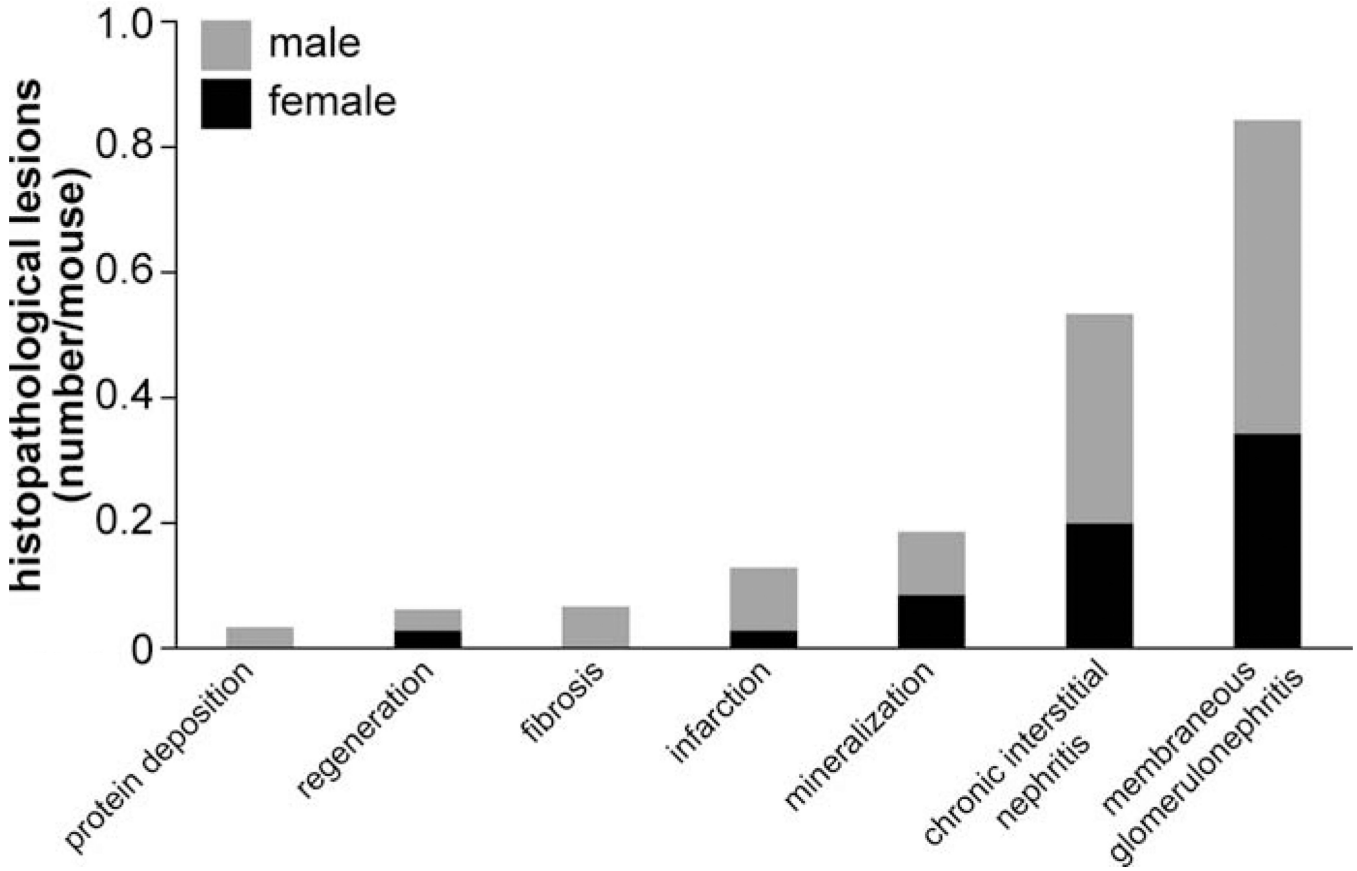

Figure 17.

Frequency of histopathological lesions in kidney. Bars show the additive number of processes for female (black) and male (gray) mice.

Table 1

Number of Mice and Histopathological Lesions at 6, 12, and 20 Months of Age and in Moribund Mice.

Characteristic	6 mo	12 mo	20 mo	Long	Total
Females					
Mice	9	15	7	4	35
Lesions	60	97	191	61	409
Lesions/mouse	7	6	27	15	12
Males					
Mice	8	12	7	3	30
Lesions	80	51	118	45	294
Lesions/mouse	10	4	17	15	10
Total					
Mice	17	27	14	7	65
Lesions	140	148	309	106	703
Lesions/mouse	8	5	22	15	11

Abbreviation: Long, longitudinal (near natural death).

Vet Pathol. Author manuscript; available in PMC 2015 February 27.

Table 2

Histopathological Diagnoses in All Examined Organs at 6, 12, and 20 Months of Age and in Moribund Mice.

		6 mo		12 mo		20 mo		Long		
Organ	**Diagnosis**	**F (9)**	**M (8)**	**F (15)**	**M (12)**	**F (7)**	**M (7)**	**F (4)**	**M (3)**	**Total**
Abdomen	Granulomatous inflammation					1				1
Abdomen	Lipid depletion							1		1
Abdomen	Lipoma							2		2
Adrenal gland	Adenoma						1			1
Adrenal gland	Hyperplasia			1		2				3
Adrenal gland	Lipofuscin deposition	1		1		3				5
Adrenal gland	Necrosis					1				1
Adrenal gland	Steatosis	2								2
Anus	Ulcer		1							1
Aorta	Vasculitis					1				1
Arterial blood vessel	Mineralization	1		2		7	1	2		13
Artery	Mineralization							1		1
Bone	Fibro-osseous lesion			6		7	1	3	1	18
Brain	Degenerative change								1	1
Brain	Dystrophy					2				2
Brain	Hydrocephalus			1		1			1	3
Brain	Mineralization			1						1
Brown fat	Mineralization			1						1
Bulbourethral gland	Ectasia								1	1
Bulbourethral gland	Mineralization						1			1
Bulbourethral gland	Protein deposition								1	1
Cecum	Acute inflammation					2				2
Cecum	Chronic inflammation					1				1
Cecum	Hyperplasia					1				1
Cecum	Ulcer					2				2
Cervical lymph nodes	Cyst						3			3
Cervical lymph nodes	Lymphoma						1			1

		6 mo		12 mo		20 mo		Long		
Organ	**Diagnosis**	**F (9)**	**M (8)**	**F (15)**	**M (12)**	**F (7)**	**M (7)**	**F (4)**	**M (3)**	**Total**
Cervical lymph nodes	Plasmacytoma					1				1
Clitoral gland	Atrophy	4		2		6		2		14
Clitoral gland	Chronic inflammation					1				1
Clitoral gland	Ectasia	4		2		7		2		15
Coagulating gland	Concretion						3			3
Colon	Hyperplasia					1				1
Ear	Acute inflammation			1		2		1	1	5
Ear	Cholesterol clefts					1				1
Ear	Concretion							1		1
Ear	Granulomatous inflammation								1	1
Ear	Mineralization						1		1	2
Esophagus	Pyogranulomatous inflammation					1				1
Eye	Adenoma			1						1
Eye	Cataract								1	1
Eye	Chronic inflammation			1				1		2
Eye	Degenerative change					1				1
Eye	Ectasia							1		1
Eye	Granulomatous inflammation					1				1
Eye	Hemorrhage and nonspecified extravasation				1				1	
Eye	Hyperplasia					5				5
Eye	Mineralization					1				1
Eye	Pigmentation			1						1
Fat	Fibrosis					1				1
Fat	Granulomatous inflammation						1			1
Gallbladder	Cholelithiasis				1					1
Gallbladder	Cyst	1								1
Hard palate	Acute inflammation			3						3
Heart	Acute inflammation					1				1
Heart	Amyloid deposition					1				1
Heart	Fatty infiltration					1				1

Vet Pathol. Author manuscript; available in PMC 2015 February 27.

		6 mo		12 mo		20 mo		Long		
Organ	**Diagnosis**	**F (9)**	**M (8)**	**F (15)**	**M (12)**	**F (7)**	**M (7)**	**F (4)**	**M (3)**	**Total**
Heart	Fibrosis					6			1	7
Heart	Mineralization	1	4	4	2	7	3	4	1	26
Hematopoietic system	Lymphoma	1	2						1	4
Intervertebral disk	Degenerative process					2	1			3
Intervertebral disk	Hernia					1				1
Jejunum	Polyp				2					2
Kidney	Chronic inflammation	1	1	3	3	3	6			17
Kidney	Fibrosis		1				1			2
Kidney	Infarction		2			3	1			6
Kidney	Membranous glomerulonephritis		3	3	3	7	7	1	2	26
Kidney	Mineralization					1	2		1	4
Kidney	Protein deposition		1			1				2
Kidney	Regeneration		1							1
Lacrimal gland	Ectasia							1		1
Lacrimal gland	Hyperplasia					1	2			3
Larynx	Acute inflammation		1							1
Leg	Acute inflammation	1								1
Lingual gland	Acute inflammation	1	1							2
Liver	Acute inflammation							1		1
Liver	Extramedullary hemopoiesis						1			1
Liver	Fibrosis	1						1		2
Liver	Granulomatous inflammation					1				1
Liver	Hepatic torsion					1				1
Liver	Hepatic tumor					1				1
Liver	Steatosis	3	3		2					8
Lung	Acute inflammation	1	1							2
Lung	Pulmonary adenoma				2					2
Lung	Fibrosis		1	1						2
Lung	Granulomatous inflammation	1								1
Lung	Mineralization			1		7	5	3	2	18

		6 mo		12 mo		20 mo		Long		
Organ	**Diagnosis**	**F (9)**	**M (8)**	**F (15)**	**M (12)**	**F (7)**	**M (7)**	**F (4)**	**M (3)**	**Total**
Lung	Subplueral pulmonary histiocytosis						1			1
Lymph nodes	Cyst			1		1				2
Lymph nodes	Hyperplasia					2				2
Lymph nodes	Plasmacytoma					1				1
Male preputial gland	Acute inflammation						1		1	2
Male preputial gland	Atrophy		7		1		6		2	16
Male preputial gland	Chronic inflammation						1			1
Male preputial gland	Ectasia		7		1		6		2	16
Male preputial gland	Granulomatous inflammation						1			1
Mammary gland	Ectasia					1				1
Mammary gland	Involution					1				1
Nasal cavity	Acute inflammation							1		1
Nasal cavity	Amyloid deposition					1				1
Nasal cavity	Concretion							1	1	2
Nasal cavity	Crystalloids chitinase-like crystals			1		2	2	1	1	7
Nasal cavity	Fibrosis								1	1
Nasal cavity	Protein deposition					3	2			5
Ovary	Atrophy					3		1		4
Ovary	Cyst					5		2		7
Ovary	Lipofuscin deposition			3		4		1		8
Ovary	Luteal cell tumor	1								1
Ovary	Mineralization					1				1
Pancreas	Acute inflammation					1				1
Pancreas	Chronic inflammation			2		1				3
Pancreas	Fatty infiltration			2	2	1				5
Pancreas	Fibrosis			4	2					6
Pancreas	Hyperplasia	8	8	15	12	7	7	1	1	59
Pancreas	Intracellular and extracellular depletion	6	4	14	12		3			39
Parotid gland	Chronic inflammation				1					1
Prostate gland	Acute inflammation						1			1

		6 mo		12 mo		20 mo		Long		
Organ	**Diagnosis**	**F (9)**	**M (8)**	**F (15)**	**M (12)**	**F (7)**	**M (7)**	**F (4)**	**M (3)**	**Total**
Salivary gland	Abscess							1		1
Salivary gland	Chronic inflammation					1				1
Seminal vesicle	Ectasia						1			1
Seminal vesicle	Mineralization						1			1
Seminal vesicle	Sarcoma						1			1
Seminal vesicle	Thrombosis						1			1
Skeletal muscle	Acute inflammation							1		1
Skeletal muscle	Degenerative change	1	1					1		3
Skeletal muscle	Fatty infiltration	4	1			3		1		9
Skeletal muscle	Granulomatous inflammation					1				1
Skeletal muscle	Hyperplasia					1				1
Skeletal muscle	Mineralization			1		1				2
Skeletal muscle	Myxosarcoma					1				1
Skin	Acanthosis							1	1	2
Skin	Acute inflammation	1	3			1			1	6
Skin	Basal cell carcinoma					1				1
Skin	Dysplasia		1							1
Skin	Dystrophy		2					1		3
Skin	Fibrosis	1					1			2
Skin	Granulomatous inflammation				2		1			3
Skin	Mineralization								2	2
Skin	Nerve sheath tumor							1	1	2
Skin	Orthokeratosis		1							1
Skin	Ulcer		2						1	3
Soft palate	Chronic inflammation						1			1
Spleen	Hyperplasia	4	1			1		3		9
Spleen	Iron deposition					3	3			6
Spleen	Melanin deposition					1				1
Spleen	Mineralization						1			1
Stomach	Acute inflammation			1						1

		6 mo		12 mo		20 mo		Long		
Organ	**Diagnosis**	**F (9)**	**M (8)**	**F (15)**	**M (12)**	**F (7)**	**M (7)**	**F (4)**	**M (3)**	**Total**
Stomach	Adenoma		1			1		1		3
Stomach	Crystalloids chitinase-like crystals		2	2		1				5
Stomach	Diverticulum					1		1		2
Stomach	Hyperplasia					1				1
Stomach	Ulcer							2		2
Teeth	Acute inflammation	1	1	2	1	6	4	2	2	19
Teeth	Avulsion								1	1
Teeth	Hyperplasia					1			1	2
Testis	Cyst		1							1
Testis	Degenerative change		2		1		7		2	12
Testis	Hyperplasia						1			1
Testis	Lipofuscin deposition						1			1
Testis	Mineralization		1				6		2	9
Testis	Telangiectasia						1			1
Thyroid gland	Cyst		1	1		1				3
Thyroid gland	Goiter						5			5
Thyroid gland	Hyperplasia					2				2
Thyroid gland	Thyroid follicle pleomorphism	2	5	2	3	2	2	3	2	21
Tongue	Acute inflammation	1	1	1						3
Tongue	Mineralization			1					1	2
Tongue	Vasculitis					1				1
Trachea	Chronic inflammation					1				1
Uterus	Acute inflammation					1				1
Uterus	Amyloid deposition	1		2		4		1		8
Uterus	Cyst	1		3				2		6
Uterus	Fibrosis					1		1		2
Vibrissa	Acute inflammation	1								1
Vibrissa	Dystrophy				1					1
Vibrissa	Mineralization	4	2	3	2	6	7	3	2	29
Total		60	80	97	51	191	118	61	45	703

Table 3

Ranges for Blood Electrolytes and the Albumin/Creatinine Ratio (ACR) Among All Strains of the Aging Studies and KK/HIJ (Females/Males).

Electrolyte	Range	6 mo	12 mo	20 mo
Calcium, mg/dl	Min	9/9	9/9	9/9
	Median	10/10	10/10	10/9
	Max	12/11	12/12	12/12
	KK	10/NA	9/10	9/10
Chloride, mmol/l	Min	105/105	111/110	110/101
	Median	116/116	116/115	115/116
	Max	123/123	124/122	125/124
	KK	114/115	114/115	113/116
Iron, mmol/l	Min	156/124	153/146	130/135
	Median	246/228	236/216	209/203
	Max	343/317	385/292	354/359
	KK	343/NA	346/260	208/196
Potassium, mmol/l	Min	5/5	5/6	5/5
	Median	6/7	6/6	6/6
	Max	7/9	7/7	8/7
	KK	6/NA	6/6	6/6
Magnesium, mmol/l	Min	2/2	2/2	2/2
	Median	3/3	3/3	2/3
	Max	3/3	3/4	4/4
	KK	3/NA	3/NA	2/NA
Sodium, mmol/l	Min	144/143	142/146	148/146
	Median	154/156	154/155	156/157
	Max	160/164	165/165	169/170
	KK	153/NA	154/152	153/156
Phosphorus, mg/dl	Min	4/5	4/4	5/5
	Median	7/7	6/7	6/7
	Max	9/10	8/9	8/9
	KK	7/NA	6/6	6/8
ACR, mg/g	Min	NA	0/0	0/0
	Median	NA	35/15	43/30
	Max	NA	484/294	974/600
	KK	NA	484/53	974/425

Abbreviations: KK, KK/HIJ; max, maximum; min, minimum; NA, not available.